TURKU-FL-R95-24
HU-TFT-95-58
hep-ph/9509359

Damping rate of neutrinos in the singlet Majoron model

Timo Holopainen [1]

Department of Physics, University of Turku, FIN-20500 Turku, Finland

Jukka Maalampi[2]

Department of Physics, Theory Division, P.O. Box 9, FIN-00014 University of Helsinki, Finland

Jukka Sirkka[3]

and

Iiro Vilja[4]

Department of Physics, University of Turku, FIN-20500 Turku, Finland

February 1, 2008

Abstract

The damping rate and free path of neutrinos in the singlet Majoron model have been calculated including both finite temperature and symmetry breaking effects. The behaviour of right- and left-handed fermions are found inherently different. While the damping rates of the left-handed leptons are essentially model independent, e.g. directly applicable to the Standard Model, for the right-handed particles the rates are crucially sensitive to parameters of the scalar sector. In general, the damping rates are fairly large. The possibility of the right-handed neutrinos to penetrate deep into the broken phase in the electroweak phase transition still remains, however, for some parts of the parameter space.

[1]tholopai@utu.fi; [2]maalampi@phcu.helsinki.fi; [3]sirkka@utu.fi; [4]vilja@utu.fi

1 Introduction

A particle traversing a thermal medium undergoes continual incoherent scatterings with plasma particles. Because of these interactions energy and momenta of the particle are not sharply defined but have a finite "width", γ. The quantity γ, called the damping rate, describes the "decay" of the state (quasiparticle) into the plasma. Only when γ is small compared with the energy will the quasiparticle propagate over meaningful distances in the plasma as a true physical excitation and with significant physical effects.

The calculation of the damping rate of quasiparticle at zero spatial momentum, $\gamma_{QCD}(0)$, in QCD plasma has been a widely disputed issue in literature [1, 2]. The controversies in the results obtained for this quantity were solved by Pisarski [2] and Braaten and Pisarski [3, 4] who developed a general method for resumming the higher loop diagrams which contribute to the damping rate in leading order.

The method of Braaten and Pisarski can be applied not only to QCD but also to other interactions. In this article we shall use it to calculate the damping rates of low momenta neutrinos in the electroweak plasma of the early universe.

We are interested in the determination of the damping rates in connection to the so-called charge transport mechanism for generating the baryon asymmetry of the universe during the electroweak phase transition [5]. This scenario is based on the assumption that the electroweak phase transition is of first order. Bubbles of the broken phase are created by fluctuations, and they grow and fill the pre-existing unbroken phase. As a bubble expands a flux of leptons from the unbroken phase hits the wall separating the phases, and some portion of the flux is reflected. As a result of violation of lepton number and C- and CP-parities, a net number of leptons is created in the unbroken phase. This is turned to a net baryon number by the sphaleron transitions. The produced baryons pass to the broken region, where baryon number is conserved, resulting in non-equal numbers of baryons and antibaryons in the universe we live.

The reflection is generally most efficient at small spatial momenta (that is why the damping rate at zero momentum is a relevant quantity to study) for the following reason. When a quasiparticle penetrates to the broken phase region it has an energy determined by the symmetric phase dispersion relation, until it begins to see the thermal background of the broken phase. If a particle has energy which is smaller than the thermal mass it acquires in the broken phase, it can propagate there only the time determined by the thermalization rate, after which it is reflected efficiently. Thermal masses are generally of the order gT, i.e. particles moving with small spatial momenta are reflected efficiently.

If its coherence length $\sim 1/2\gamma$ is small compared with its effective reflection length,

a typical quasiparticle decays into the plasma before it is reflected. This would suppress the generation of the baryon number making the scenario less viable. Actually, it has been claimed [6, 7] that in the picture where the baryon number is created, instead of neutrinos, by a reflection of quarks from the phase boundary, this is what happens: decoherence effects crucially diminish the baryon number creation. It is interesting to investigate what is the situation with neutrinos. In the present paper we will calculate the damping rates for left-handed and right-handed neutrinos in the Majoron model. The consequences of the result with respect to the baryon number generation will be analyzed in a separate publication [8].

The organization of the paper is the following. In Section 2 we will introduce the model we are working with, the singlet Majoron model. In Section 3 we derive the effective vertices and propagators, and in Section 4 we apply them to the calculation of the zero momenta damping rates. The numerical results are presented in Section 5, and the conclusions drawn in Section 6.

2 The singlet Majoron model

For evaluating the neutrino damping rate one has to specify the model. We will use the singlet Majoron model [9], which is an extension of Standard Model containing an extra gauge singlet scalar field S, as well as gauge singlet right-handed neutrinos. The lagrangian of the model is the most general one with the requirement that it has a global $B-L$ symmetry. Spontaneous breaking of this global symmetry by a non-vanishing vacuum expectation value (vev) of the singlet scalar, $\langle S\rangle = \bar{f}$, generates Majorana masses to the neutrinos. The see-saw mechanism can be implemented yielding three neutrinos which are very light compared with the other fermions of the model and three neutrinos which are very heavy. It is usually assumed, to avoid an ad hoc hierarchy among the energy scales, that $\bar{f}$ is comparable in size with the vev $\langle\Phi\rangle = f$ of the ordinary doublet Higgs Φ responsible on the electroweak symmetry breaking. The model can fulfill the Sakharov conditions [10] for the creation of a cosmological asymmetry between baryons and antibaryons, as was demonstrated in [5].

The singlet Majoron model contains the following new Yukawa interactions not present in the Standard Model:

$$\mathcal{L}_Y = \overline{l}_L \lambda_D \tilde{\Phi} N_R + \overline{N}_R \lambda_M S N_L^c. \tag{1}$$

Here $\tilde{\Phi}$ is the conjugate of the Higgs doublet, l_L is a vector of left-handed lepton doublets and N_R is a vector of right-handed singlet neutrinos. The Yukawa coupling matrices λ_D and λ_M are in general non-diagonal in flavor space.

The first term of (1) gives rise to Dirac masses and the second term to Majorana masses for neutrinos. In order to satisfy the experimental mass limits of the known

neutrinos one has to require, given our assumption that there is no strong hierarchy between the vevs f and $\bar{f}$, that the elements of λ_D are much smaller than the elements of λ_M, so as to make the predominantly left-handed neutrinos very light. A detailed discussion of the masses, mixings and phase transitions in the singlet Majoron model can be found in [11]. We just note that due to a large number of free parameters appearing in the model and a lack of constraining experimental data, the vacuum expectation value $\bar{f}$, singlet scalar mass and Majorana masses can be considered as practically free parameters.

3 Effective vertices and propagators

The damping rate is defined as the imaginary part of the solution $\omega = \omega(k)$ of the dispersion relation

$$\det\left(\Delta_f^{-1}(\omega, \mathbf{k})\right) = \det\left(\omega\gamma^0 - \mathbf{k}\cdot\boldsymbol{\gamma} - \Sigma(\omega, \mathbf{k}) - m_f\right) = 0, \tag{2}$$

where Δ_f is the fermion propagator, Σ is the fermion self-energy and m_f is the vacuum mass of the fermion. The contributions to the finite temperature self-energies that one has to consider in order to determine the zero momentum damping rate of the Majorana neutrinos in the singlet Majoron model are displayed in Fig. 1. In this section we shall outline the computation of the effective propagators and vertices (presented by the 'blobs') out of which these amplitudes are constructed. In the next section we will apply the results to evaluate the damping rates. In our calculation we will make the following approximations. We will compute all quantities in leading order in coupling constants, neglect the Yukawa couplings except the Majorana couplings of the right-handed neutrinos, and when necessary take subleading terms into account to avoid problems with infrared divergent graphs.

We will apply the method of Braaten and Pisarski [3] to identify those higher-loop diagrams, called hard thermal loops (HTL), which contribute in leading order and which are necessary for the gauge invariance of the damping rate. By definition, HTL's are those diagrams which contribution to effective vertices is of the same order in coupling constants as the contribution of the tree level diagrams. According to [3], an amplitude contributing the effective vertices and propagators can be an HTL only when its external legs are all soft, i.e. the momenta of the external particles are of the order $\sim gT$, where T is temperature and g is a generic coupling constant.

Let $P = (p_0, \mathbf{p})$ denote the external soft momentum and $K = (k_0, \mathbf{k})$ the loop momentum. Whether a given amplitude is an HTL can be determined by applying the power counting rules introduced in Ref. [3]: the integration element $\int d^3k$ contributes T^3; the first propagator in the loop and the summation over k_0 together contribute $1/T$, and all other propagators give a contribution $1/(PT)$ each; K^μ in the numerator

contributes T; P^μ in the numerator contributes gT; for loop where internal lines are all bosonic or fermionic there is an extra factor of P/T.

The hard part of an amplitude corresponds to making a linear approximation in the external momentum $P \sim gT$ in propagators, i.e. neglecting P^2 as small compared with $P \cdot K$. The particle masses, which appear in the propagators quadratically, can be neglected, because they are generally of the order gv, where v is a generic vacuum expectation value of a symmetry breaking Higgs boson and g is a generic coupling. An exception seems to be scalar masses, which are lower order in coupling constant, $m_S^2 \sim gv^2$. However, perturbatively in finite temperature one has $v \sim g^{1/2}T$, and since the soft scale of scalar lines should be identified with $\sim g^{1/2}T$, we can neglect in leading order also the scalar masses in loops. For example, calculating the scalar tadpole diagram, which arises from scalar self-coupling, gives for the scalar a thermal mass $\sim g^{1/2}T$, which is small compared with the relevant loop momentum.

Let us now move to consider in one loop level the effective two-point, three-point and four-point functions entering the diagrams of Fig. 1. There is obviously a great number of loop diagrams contributing, but it turns out that just a handful of them are HTL's and thus relevant in leading order evaluation of the damping rates. We will not go through our analysis in full detail diagram by diagram here, but rather just describe the general methods we have used to discard the amplitudes yielding a non-leading contribution and to pick up the HTL's.

Let us first consider diagrams for the left-handed neutrinos. In the case of the gauge boson - neutrino pair three-point function there are five different types of diagrams, which may be conveniently classified according to the types of their internal lines. Let F denote a fermion line, S a scalar line and A a gauge boson line. The diagrams with configurations FFA and FAA have good infrared behaviour. They are HTL's, and the calculation of them is presented in the Appendix. The diagrams FFS and FSS have also good infrared behaviour and they are HTL's, but because they contain small Yukawa couplings we neglect them. The configuration FAS has a vertex V(AAS) which originates in the symmetry breaking and which has with a coupling proportional to $g^2 f$. By the power counting rules its contribution would be $\sim g^2 f/T$, i.e. of higher order than the tree level contribution. However, due to the behaviour of this graph in the infrared region, its contribution is larger than given by the pure power counting argument. To see this, and to introduce our scheme to approximate the contributions from the infrared integration regions, let us consider the amplitude FAS in more detail.

Using the standard imaginary time formalism [12] to perform the summation over discrete loop energy (see also Appendix), the diagram FAS may be cast into the form

$$\Gamma(\mathrm{FAS}) \sim g^4 f \int \frac{d^3k}{(2\pi)^3} \left[K \cdot \gamma|_{k_0=\omega_k} \frac{f_B(\omega_k)}{2\omega_k} \frac{1}{(\omega_k + p_1^0)^2 - \omega_{k+p_1}^2} \frac{1}{(\omega_k + p_2^0)^2 - \omega_{k+p_2}^2} + \ldots \right]. \tag{3}$$

Here $\omega_{k+p}^2 = (\mathbf{k}+\mathbf{p})^2 + m^2$, f_B is the Bose-Einstein distribution function, the P_i's are some combinations of the external momenta, and m is the mass of the loop particle. The external energies p_i^0 are here continued to real values. If one makes a linear approximation in the external four-momenta and neglects the masses in denominators, the integral in (3) becomes infrared divergent and it behaves as

$$\Gamma(\mathrm{FAS})_{\mathrm{IR}} \sim g^4 f \int \frac{dk}{k}\frac{T}{P^2} = g^2 \frac{f}{T}\int \frac{dk}{k}, \tag{4}$$

where P denotes generically the soft external momentum scale. As the integral is only logarithmically divergent the contribution from the infrared region is of the order of $g^2\log(g)f/T$. Hence $\Gamma(FAS)$ is not an HTL in spite of its divergent infrared behaviour.

By generalizing previous example one obtains power counting rules for the infrared region: the summation over k_0 and one propagator contributes together treating $1/(gT)$; the integration element d^3k contributes $(gT)^3$; the loop momentum K is taken to be of the order of the external soft momentum $P \sim gT$ both in the nominator and in the denominator; and the Bose-Einstein distribution function contributes $1/g$.

There are five types of diagrams contributing to the scalar-fermion pair three-point function: FFA, FFS, FAS, FAA and FSS. All but one, FAA, of these configurations contain small Yukawa couplings, and hence we shall neglect them. The diagram FAA is due to the symmetry breaking, and it behaves as $\sim g^2 f/T$ both in the ultraviolet and infrared regions. Because also the tree level coupling of the left-handed neutrinos and a scalar is proportional to small Yukawa coupling, the effective scalar – neutrino pair vertex can be omitted for the left-handed neutrinos altogether.

A note concerning the configuration FSS is in order. It contains a scalar three point vertex arising through the symmetry breaking from the scalar four-point coupling, generically denoted by λ, of the symmetric theory. Power counting results in a contribution $\sim gv/T$, where v is a generic vacuum expectation value parameter. Thus if v is of the same order than temperature T, one should consider the FSS diagram as a HTL. But here one should be careful to check whether the contribution comes from the scalar or from the fermion line (see Eq. (A10)). By identifying the soft scale of the scalars with $\lambda^{1/2}T$, these contributions are $\sim g_Y^2 v/T$ and $\sim \lambda^{1/2} g_Y v/T$, respectively. Here g_Y is a generic Yukawa coupling. One can check that also the ultraviolet region gives a subleading contribution and hence FSS diagram is not an HTL. Formally the same result is achieved if $\lambda^{1/2}$ is considered as the perturbation parameter of the scalar sector.

With the above note in mind one can check that from the 13 possible diagrams of the two gauge boson – neutrino pair four-point function only three, FAAA, FFAA and FFFA, contribute. The calculation of these is outlined in the Appendix. There are five diagrams which have vertices arising from the symmetry breaking: FFAS; two diagrams of the type FASS; two diagrams of the type FAAS (these are neglected

because they are not HTL's); two non-HTL diagrams with vertices of the symmetric theory: FAA and FSS; and three diagrams containing small Yukawa couplings: FSSS, FFSS and FFFS.

Further one can check that none of the 13 possible diagrams of the two scalar – neutrino pair diagrams contribute. There are six diagrams with symmetry breaking vertices: FSSS, FAAS, FAAA, FASS, FFSS and FFAA; these are again neglected because their are not HTL's; three non-HTL diagrams of the symmetric theory: FAAS, FSS and FAA; and four diagrams of the symmetric theory containing small Yukawa couplings: FASS, FFAS, FFFS and FFFA.

Finally, none of the three possible diagrams FFSS, FFAS and FFAA contributes to the effective four neutrino vertex [4]. Thus we are left with the effective contributions to the self-energy of the left-handed neutrino of Fig. 1 a.

Similar considerations of the effective vertices entering to the calculation of the self-energy of the right-handed neutrino are much more simpler because the particle is a gauge singlet: there are no three-point or four-point functions of right-handed neutrino pair and gauge bosons.

The three-point function of a right-handed neutrino pair and a scalar has two possible one loop contributions: the diagrams FFS and FSS. The latter is not HTL by the argument applied already in the left-handed case. The former is neither HTL: the fermion propagators produce a term K^2 to the denominator of the integrand of the diagram and hence cancel corresponding factor in the nominator. Effectively this gives an extra factor of g to the order this diagram. Thus the effective three point function of the right-handed neutrino pair and a scalar consists just of the tree level term.

The four-point function of a right-handed neutrino pair and two scalars has four possible one loop contributions: the diagrams FSSS, FSS, FFSS and FFFS. The first two of these are non-HTL diagrams by power counting, while the third and the fourth are not HTL diagrams because of the K^2 term in the denominator due to the fermion propagators.

Finally, similarly as in the case of the case of left-handed neutrinos the possible contribution FFSS to the four neutrino vertex is not a HTL. Thus we are left with the effective contribution to the self-energy of the right-handed neutrino of Fig. 1 b. The effective neutrino pair – scalar three point function consists only of the tree level contribution.

The two-point functions which contribute to the effective propagators of left- and right-handed neutrinos, scalars and gauge bosons are selected correspondingly. It turns out that only the diagrams of the symmetric theory contribute in leading order. Further, in the case of left-handed fermions, because of the negligible Yukawa couplings, only the diagram of the type FA contributes and, in the case of right-handed neu-

trinos, being gauge singlets, only the diagram FS contributes. In the case of scalars the two-point function is independent of the external momentum and it just gives a contribution to the mass term of the scalars.

The effective, high-temperature, two-point functions of the gauge bosons and fermions are well known (see e.g. Refs. [13, 15]). They are listed in the Appendix.

4 Zero momentum damping rate

The neutrino damping rates at zero momentum are calculated to leading order by evaluating the one-loop diagrams of Figs. 1 a and 1 b, where the effective couplings and propagators include the hard thermal loops discussed in the previous Section. We will consider the damping rates of the left-handed neutrinos and right-handed neutrinos, that is, of the light and heavy Majorana neutrinos, separately. There is an essential difference between these two cases because the interactions of the two sets of particles differ.

4.1 Left-handed neutrinos

In the left-handed sector, according to the analysis of the previous Section, only the graphs of unbroken gauge theory contribute. Thus the calculation of effective n-point functions proceeds similarly as in the case of QCD [4], except that the group theoretical factors are replaced by those corresponding to the $SU(2)\times U(1)$ symmetry, and one has to take into account the left-handed nature of neutrinos, as well as the scalar doublet contribution to the gauge boson thermal masses. Although the modifications to the QCD results are quite straightforward, we present for completeness some technical details in Appendix.

We wish to study the leading symmetry breaking effects, that is, an inclusion of the vacuum mass terms of gauge bosons, to the zero momentum damping rate of light neutrinos. Although the diagrams arising from the spontaneous symmetry breaking were neglected as subleading when the effective vertices were calculated, the gauge boson and fermion masses created through the symmetry breaking, so-called vacuum masses, may have as important effects to the damping rate as the thermal masses arising from the interactions with the plasma. One should note that the inclusion of the vacuum mass terms does not spoil the gauge invariance of the damping rates, since the Ward identities obeyed by the n-point functions remain unaltered [3]. These identities guarantee that the gauge dependent piece of the gauge boson propagator gives zero contribution to the on-shell damping rate. The relevant identities are displayed in Appendix.

The effective self-energy of a left-handed neutrino may be written as

$$\Sigma^{(1)}(P) = T\sum_{k_0}\int\frac{d^3k}{(2\pi)^3}\Big[\Gamma^A_\mu(P,P-K)\Delta_l(P-K)\Gamma^B_\nu(P,P-K)G^{\mu\nu}_{AB}(K) + \tfrac{1}{2}\Gamma^{AB}_{\mu\nu}(P,K)G^{\mu\nu}_{AB}\Big]. \quad (5)$$

Here Γ^A_μ is the effective gauge boson – neutrino pair three-point function, $\Gamma^{AB}_{\mu\nu}$ is the effective four-point vertex for neutrinos and gauge bosons, Δ_l is the effective propagator of a left-handed neutrino, and $G^{\mu\nu}_{AB}$ is the effective propagator of gauge bosons. The indices A, B refer to the $SU(2)\times U(1)$ gauge bosons.

The gauge boson propagator may be divided into longitudinal and transverse projections [13]:

$$G^{AB}_{\mu\nu}(K) = \Delta^{AB}_T\hat{P}_{\mu\nu} + \Delta^{AB}_L\hat{Q}_{\mu\nu}, \quad (6)$$

where $\hat{P}_{\mu\nu}$, $\hat{Q}_{\mu\nu}$ together with $\hat{K}_{\mu\nu} = k_\mu k_\nu/K^2$ form a set of projection operators obeying $\hat{P}_{\mu\nu}+\hat{Q}_{\mu\nu}+\hat{K}_{\mu\nu} = g_{\mu\nu}$. Explicitly,

$$\hat{P}_{\mu\nu} = g_{\mu\nu} - U_\mu U_\nu + \frac{1}{k^2}(K_\mu - k_0U_\mu)(K_\nu - k_0U_\nu), \quad (7)$$

where $U = (1,0,0,0)$ is the four-velocity of the plasma. The gauge dependent part, which is proportional to $\hat{K}_{\mu\nu}$, is not displayed in Eq. (6). The longitudinal and transverse propagators $\Delta_{L,T}$ have the form

$$\Delta^{AB}_{L,T}(k) = \Big(K^2 - M^2 - \Pi_{L,T}(K)\Big)^{-1}_{AB}, \quad (8)$$

where M^2 is the vacuum mass matrix, and $\Pi_{L,T}$ are the longitudinal and transverse projections of the vacuum polarization tensor.

The damping rate is defined as the imaginary part of the effective self-energy, which one finds as the solution of the dispersion relation. It reads at zero momentum as follows:

$$\begin{aligned}\gamma(0) &= \frac{1}{8}\mathrm{Tr}\left(\gamma_0\,\mathrm{Im}\,\Sigma^{(1)}(p_0=\omega_l,\mathbf{p}=0)\right)\\ &= \frac{1}{16i}\,\mathrm{Disc}\,\mathrm{Tr}\left(\gamma_0\Sigma^{(1)}(p_0=\omega_l,\mathbf{p}=0)\right).\end{aligned} \quad (9)$$

The operation $\mathrm{Disc}\,f(x) \equiv f(x+i0^+) - f(x+i0^-)$ extracts the disconnected part of the function f, and ω_l is the thermal mass of the left-handed neutrino. After some tedious algebra, we may write the damping rate to the form

$$\gamma(0) = \frac{1}{i}\,\mathrm{Disc}\,T\sum_{k_0}\int\frac{d^3k}{(2\pi)^3}\left[\frac{1}{2}\{F_A,F_B\}\Delta^{AB}_T\Gamma_T + \frac{1}{2}\{F_A,F_B\}\Delta^{AB}_L\Gamma_L\right], \quad (10)$$

where F_A and F_B are group generators (multiplied with the corresponding gauge coupling constant) and

$$\begin{aligned}
\Gamma_L &= -\frac{K^2}{k^2}\frac{1}{\omega_l^2}\frac{1}{2}\sum_{\pm}\Delta_{\pm}(P-K)\left(\omega_l+p_0-k_0\mp k\right)^2, \\
\Gamma_T &= -\frac{1}{4\omega_l^2}\sum_{\pm}\Delta_{\pm}(P-K)\frac{1}{k^2}\left[(p_0-k_0)^2-(k\pm\omega_l)^2\right]^2 \\
&\quad +\frac{1}{4k}\left(1-\frac{(p_0-k_0)^2}{k^2}\right)\ln\left(\frac{p_0-k_0-k}{p_0-k_0+k}\right). \qquad (11)
\end{aligned}$$

The neutrino propagator is here divided into the helicity components $\Delta_{\pm}$,

$$\Delta_l(P)=\frac{1}{2}\Delta_+(\gamma^0-\hat{\mathbf{p}}\cdot\boldsymbol{\gamma})+\frac{1}{2}\Delta_-(\gamma^0+\hat{\mathbf{p}}\cdot\boldsymbol{\gamma}). \qquad (12)$$

The form Eq. (10) is similar to the QCD case [3], only that the gauge boson propagator factors have now a more complicated form.

The sum over the discrete loop energy values may be performed with the help of the formula

$$\begin{aligned}
&\mathrm{Disc}\,T\sum_{k_0}B(k_0)F(p_0-k_0)_{|_{p_0=E}}= \\
&2\pi i\left(e^{E/T}+1\right)\int_{-\infty}^{\infty}d\omega f_B(\omega)\rho_B(\omega)\int_{-\infty}^{\infty}d\omega' f_F(\omega')\rho_F(\omega')\delta(E-\omega-\omega'), \qquad (13)
\end{aligned}$$

where the argument of the function B (F) is even (odd) multiple of $\pi T i$, $f_{B(F)}$ is the Bose-Einstein (Fermi-Dirac) distribution, $\rho_B(\omega)=1/(2\pi i)\mathrm{Disc}\,B(\omega)$ is the spectral function of $B(\omega)$ and ρ_F is similarly the spectral function of $F(\omega)$.

The damping rate of the left-handed neutrino in the zero momentum limit is thus given by the formula

$$\gamma(0)=\frac{g_2^2T}{16\pi}\,a, \qquad (14)$$

where

$$\begin{aligned}
a &= \frac{e^{\omega_l/T}+1}{\omega_l^2}\int k^2dk\,d\omega\,d\omega'\delta(\omega_l-\omega-\omega')f_F(\omega')\frac{\omega}{T}f_B(\omega)\times \\
&\quad \left[\frac{2\rho_L(\omega,k)}{\omega}\sum_{\pm}\rho_{\pm}(\omega',k)\left(\omega_l+\omega'\mp k\right)^2+\frac{\rho_T(\omega,k)}{\omega}\times\right. \\
&\quad \left.\left(\sum_{\pm}\rho_{\pm}(\omega',k)\frac{1}{k^2}\left(\omega'^2-(k\pm\omega_l)^2\right)^2+\frac{k^2-\omega'^2}{k^3}\omega_l^2\theta(k^2-\omega'^2)\right)\right], \qquad (15)
\end{aligned}$$

and

$$\begin{aligned}
\rho_L &= \frac{\mathrm{Disc}}{2\pi i}\left[\frac{1}{2g_2^2}\{F_A,F_B\}\Delta_L^{AB}(\omega,k)\frac{\omega^2-k^2}{k^2}\right], \\
\rho_T &= \frac{\mathrm{Disc}}{2\pi i}\left[\frac{1}{2g_2^2}\{F_A,F_B\}\Delta_T^{AB}(\omega,k)\right], \\
\rho_{\pm} &= -\frac{\mathrm{Disc}}{2\pi i}\left[\Delta_{\pm}(\omega',k)\right]. \qquad (16)
\end{aligned}$$

Here g_2 is the $SU(2)$ gauge coupling.Note that Eq. (15) applies for the both components of the left-handed lepton doublet, the neutrino and the charged lepton, by choosing the appropriate T_3 quantum number.

The gauge boson spectral functions separate naturally to the W-boson, Z-boson and photon terms:

$$\frac{\rho_{L,T}(\omega,k)}{\omega} = \sum_{K=\gamma,Z,W} Z^K_{L,T}(k)\left(\delta(\omega-\omega^K_{L,T}(k))+\delta(\omega-\omega^K_{L,T}(k))\right)+\theta(k^2-\omega^2)R_{L,T}(\omega,k), \tag{17}$$

where the delta-function terms arise from the poles of the propagators $\Delta_{L,T}$ and the step function term from the cut $k^2>\omega^2$ of the logarithmic terms in the propagators. The explicit expressions of these are straightforward to calculate, resulting, however, in rather lengthy formulas not displayed here. Similarly, the fermion spectral functions $\rho_\pm$ may be expressed as

$$\rho_\pm(\omega,k) = Z_+(k)\delta(\omega\mp\omega_+(k))+Z_-\delta(\omega\pm\omega_-(k)+\theta(k^2-\omega^2)R_\pm(\omega,k) \tag{18}$$

with $R_-(\omega,k)=R_+(-\omega,k)$.

Following Ref. [15], the residues $Z^{\gamma,Z,W}_{L,T}$ and $Z_\pm$ may be interpreted as probabilities of creating an excitation obeying the energy-momentum dispersion relation $\omega=\omega^{\gamma,Z,W}_{L,T}(k)$ and $\omega=\pm\omega_\pm(k)$ in the plasma, respectively. In the case of fermions we may interpret the two branches $\pm\omega_\pm$ as particle-like and hole-like excitations. The negative-energy solutions are interpreted as antiparticles as usual. Further, the coefficient of the step function may be interpreted as the contribution of the particles in the heat bath to the spectral functions: the quasiparticles are not strictly on mass shell, because they interact with the heat bath.

With these interpretations, one may divide the coefficient a into separate contributions according to whether the energies ω and ω' in Eq. (15) are off-shell or on-shell. Particularly, if the both energies are on-shell, the corresponding contributions are interpreted as processes $\nu_p\, l_h \to A$ and $\nu_p\, \bar{l}_p \to A$, where A denotes generically one of the bosons γ, Z or W, l denotes generically the left-handed doublet lepton, and subscripts p and h refer to particle and hole excitations, respectively [16]. The other possible processes are kinematically forbidden, and it is easy to show that the processes above are allowed only if the thermal mass of the boson is larger than $2\omega_l$. Note that the hole excitation has same quantum numbers as the anti-particle excitation but the opposite helicity [15].

In addition to the on-shell contribution there are contributions where at least one of the particles in the loop in Fig. 1 a is off-shell. These contributions may be interpreted as due to the interactions of the quasiparticles with the heat bath. The behaviour of the integrand in Eq. (15) for these contributions is such that the main contribution to a comes from the soft region. In that case one can approximate $\exp(\omega_l/T)\simeq 1$,

$f_B(\omega) \simeq T/\omega$ and $f_F(\omega') = 1/2$. The result is that the parameter a is independent of temperature (the same is the case in QCD [4]). The on-shell contribution is exceptional: schematically it reads

$$a_{\rm OS} = \frac{Z_{L,T}(k_0)Z_{\pm}(k_0)}{|\omega'_{\pm}(k_0) - \omega'_{L,T}|} f_F(-\omega_{\pm}(k_0)) f_B(\omega_L, T(k_0)) \times (\ldots), \tag{19}$$

where k_0 is the solution to the equation $\omega_l + \omega_{\pm}(k) - \omega_{L,T}(k) = 0$, prime denotes derivation and the ellipsis represent contributions that are not relevant in our reasoning. It can be shown that Z_T and Z_+ approach unity when k increases, while Z_L and Z_- approach zero exponentially. Further, ω_T and ω_+ approach the free particle dispersion relation $\omega = (k^2 + M^2)^{1/2}$, M is the vacuum mass, with increasing k, while ω_L and ω_- approach the massless dispersion relation $\omega = k$ exponentially. Consider the case of transverse boson and particle-like neutrino excitations in Eq. (19). If the vacuum mass of the gauge boson is large, $M \gg \omega_l$, then $k_0 \approx M^2/(2\omega_l)$ and

$$a_{\rm OS} \sim \frac{M^2}{\omega_l^2} e^{-k_0/T}, \tag{20}$$

which means that without Boltzmann suppression a would grow to high values with increasing $f \sim M$.

4.2 Right-handed neutrinos

The calculation of the zero momentum damping rates of right-handed neutrinos proceeds along the same lines as of the left-handed ones, the main difference being the inclusion of the vacuum mass term to the propagator of the right-handed neutrino. According to the analysis of the previous section we need to calculate the disconnected part of the diagram in Fig. 1 b. In the case of right-handed neutrinos the three-point vertex is bare; there is no HTL-contribution to it. Furthermore, as mentioned in the previous Section, the HTL-contributions to the scalar self-energies are independent of the external soft momentum P. They merely add a contribution to the mass term of scalars, which is, in fact, already taken into account when we use the temperature corrected scalar potential.

The evaluation of the effective self-energy Σ_R of the right-handed neutrinos follows the same lines as that of the left-handed neutrinos. The only change is the replacement of the squared thermal masses with

$$\omega_r^2 = \lambda_M \lambda_M^{\dagger} \frac{T^2}{16}. \tag{21}$$

Because we assume that the Dirac mass terms connecting the left- and right-handed neutrinos are neglected as compared with the Majorana mass terms, the vacuum mass

terms and the thermal energies are diagonalized simultaneously. The effective lagrangian can then be presented in the mass eigenstate basis as follows:

$$\mathcal{L}_{eff} = \frac{1}{2}\overline{\chi}_l \left(\gamma \cdot P - \Sigma_L\right) \chi_l + \frac{1}{2}\overline{\chi}_h \left(\gamma \cdot P - \Sigma_R^d - m_M\right) \chi_h + \cdots \tag{22}$$

Here χ_l and χ_h represent the light (mainly left-handed) and heavy (mainly right-handed) mass eigenstates of neutrinos, respectively. The self-energies Σ_L and Σ_R^d are diagonal. Thermal masses of the the heavy flavour eigenstate neutrinos are (i=1,2,3)

$$m_{R,i}^2(T) = \frac{T^2}{32\bar{f}^2} m_{M,i}^2. \tag{23}$$

Here $m_{M,i}$ is the vacuum mass given by $\sqrt{2}\bar{f}\lambda_{M,ii}^{\rm diag}$, where $\lambda_M^{\rm diag}$ is the diagonalized form of the coupling matrix of the right-handed neutrinos and the singlet scalar defined in Eq. (1).

The vacuum mass terms of the scalars give rise to a mixing between the singlet Higgs and the neutral member of the Higgs doublet. Hence the scalar propagator appearing in the neutrino self-energy amplitudes is a 2×2 matrix. The component of this matrix corresponding to the dominant channel to which heavy neutrinos couple with a large Yukawa coupling is given by

$$\frac{\Gamma_{hh}}{\Gamma_{hh}\Gamma_{ss} - \Gamma_{hs}^2}. \tag{24}$$

Here $\Gamma_{hh} = K^2 - m_{hh}^2(T)$ and $\Gamma_{ss} = K^2 - m_{ss}^2(T)$ are the inverse propagators of scalars h and s, and Γ_{hs} is the mass mixing term arising from the scalar potential through the symmetry breaking. Subscripts h and s refer to the neutral, P-even components of the doublet and singlet fields, respectively. As a matter of fact, one can neglect in (24) the scalar mass mixing term Γ_{hs}. As will be seen in the next Section, inclusion of it would play subdominant role as compared with the much more substantial effects of the inclusion of the vacuum mass term of the right-handed neutrino. In addition to the scalar contribution in Eq. (24), there is also a Majoron contribution.We shall neglect the thermal mass differences of the Majoron and the other scalars, and combine the effects of these particles by using a complex scalar field S to describe the scalar degrees of freedom.

Unlike for the left-handed neutrinos, the zero momentum damping rates for the particle- and hole-like excitations differ in the case of the right-handed neutrinos as a result of the inclusion of the vacuum mass term. Namely, the imaginary part of the self-energy $\Sigma_R^{(1)}$ at zero spatial momentum has two contributions α_1 and α_2 defined through

$$\mathrm{Im}\,\Sigma_R^{(1)}(p_0 = \omega_r^{\pm}, \mathbf{p} = 0) = \alpha_1^{\pm}\gamma^0 + \alpha_2^{\pm}, \tag{25}$$

where

$$\omega_r^{\pm} = (m_R(T)^2 + \frac{1}{4}m_M^2)^{1/2} \pm \frac{1}{2}m_M, \tag{26}$$

are the thermal masses of the particle (+ sign) and the hole (- sign) excitations in the case of nonvanishing vacuum mass. From the zero momentum dispersion relation

$$\left(p_0 - \frac{m_R(T)^2}{p_0} - i\alpha_1\right)^2 - (m_M + i\alpha_2)^2 = 0 \tag{27}$$

one may then deduce that the zero momentum damping rates $\gamma_{\pm}(0)$ of the right-handed neutrinos read

$$\gamma_{\pm}(0) = \frac{1}{2}(\alpha_1^{\pm} \pm \alpha_2^{\pm}). \tag{28}$$

Similarly as in the left-handed calculation the damping rates can be written in the form

$$\gamma_{\pm}(0) = \frac{|\lambda_M^{diag}|^2 T}{16\pi} a_{\pm}, \tag{29}$$

where

$$\begin{aligned} a_{\pm} &= 4(e^{\omega_r^{\pm}} + 1) \times \int k^2 dk \int d\omega d\omega' \delta(\omega_r^{\pm} - \omega - \omega') \\ &\quad \frac{\omega}{T} f_B(\omega) f_F(\omega') \frac{\rho_S(\omega, k)}{\omega} \left(\rho_{r1}(\omega', k) \pm \rho_{r2}(\omega', k)\right). \end{aligned} \tag{30}$$

Here the scalar spectral function ρ_S has a very simple form:

$$\frac{\rho_S(\omega, k)}{\omega} = \frac{1}{2\omega_S^2(k)} \left(\delta(\omega - \omega_S(k)) + \delta(\omega + \omega_S(k))\right), \tag{31}$$

where $\omega_S(k) = (k^2 + m_S(T)^2)^{1/2}$. The neutrino spectral function contains two parts, ρ_{r1} and ρ_{r2}, corresponding to the imaginary parts $\alpha_{1,2}$ in Eq. (25). The right-handed neutrino propagator may be written in the form

$$\begin{aligned} \Delta_R(P) &= (f(p_0, p)\gamma_0 + h(p_0, p)\hat{\mathbf{p}} \cdot \boldsymbol{\gamma} - m_M)^{-1} \\ &= \frac{1}{f^2(p_0, p) - h^2(p_0, p) - m_M^2} \left(f(p_0, p)\gamma_0 + h(p_0, p)\hat{\mathbf{p}} \cdot \boldsymbol{\gamma} + m_M\right), \end{aligned} \tag{32}$$

where functions f and h are defined through Eqs. (A23) and (A24). One can then write the spectral functions ρ_{r1} and ρ_{r2} as follows:

$$\begin{aligned} \rho_{r1}(\omega, k) &= \frac{\text{Disc}}{2\pi i}\left[\frac{f(\omega, k)}{f^2(\omega, k) - h^2(\omega, k) - m_M^2}\right], \\ \rho_{r2}(\omega, k) &= \frac{\text{Disc}}{2\pi i}\left[\frac{m_M}{f^2(\omega, k) - h^2(\omega, k) - m_M^2}\right]. \end{aligned} \tag{33}$$

Factorization to the helicity components is not possible in the case of the right-handed neutrino propagator because of the vacuum mass term. However, as before

the propagator has four poles $\omega = \pm\omega_r^{\pm}(k)$, which may be interpreted as dispersion relations of the particle-, antiparticle-, hole- and antihole-like excitations, but in contrast with the vanishing vacuum mass limit there are now two residues corresponding to the two contributions to the spectral functions ρ_{r1} and ρ_{r2}. Similarly there are also two off-shell contributions proportional to the step function $\theta(k^2 - \omega^2)$.

The on-shell channels contributing the damping rates are listed in Table 1. Similarly as in the calculation concerning the left-handed neutrinos, the on-shell contribution to the parameter $a_\pm$ may be written schematically as

$$a_{\pm,\mathrm{OS}} = \frac{Z_{1,2}^{\pm}(k_0)}{|\omega'_{\pm}(k_0) \pm \omega'_S(k_0)|} f_F(\pm\omega_r^{\pm}(k_0)) f_B(\pm\omega_S(k_0)) \times (\ldots), \tag{34}$$

where k_0 is the solution of the equation $\omega_r^{\pm} \pm \omega_r^{\pm}(k) \pm \omega_S(k) = 0$. The sign choices depend on the channel in question. Again, the residue terms $Z_{1,2}$ for particle excitations only are non-negligible for large k_0. Further, the denominator in Eq. (34) approaches zero for large k_0, if there is a relative minus sign between the two derivatives $\omega'_{\pm}(k_0)$ and $\omega'_S(k_0)$. These two conditions are fulfilled in the case of the particle damping rate for the channel $\nu_p\bar{\nu}_p \to S$ and in the case of the hole damping rate for the channels $\bar{\nu}_h S \to \nu_p$ and $\bar{\nu}_h\bar{\nu}_p \to S$. These channels give the largest contributions to the damping rates, as is evident from Figures 3 and 4.

5 Numerical results

The zero temperature damping rates left- and right-handed neutrinos derived in the previous section have quite complicated analytic form. In this section we analyze their properties numerically. Instead of the damping rates themselves we will present in our plots the coefficients a and $a_\pm$ defined in Eqs. (14) and (29).

In Fig. 2 we have plotted the coefficient a, which is proportional to the damping rate of the left-handed neutrinos, as a function of the vacuum expectation value f of the doublet Higgs. As can be seen from the figure, a is essentially independent on f. This result can be understood due to the fact that, although the vacuum mass does suppress the damping rate, there is now a new thermalization channel open, which has no counterpart e.g. in the pure QCD case [4]. The annihilation of the left-handed neutrino with a neutrino from the heat bath namely gives a large contribution to the rate. In fact, its contribution increases with increasing f, in contrast with all the other contributions which decrease. For $f/T \sim 1.4$ it corresponds to about a half of the whole rate. For very larger values of f, however, also this annihilation contribution starts to diminish due to Boltzmann suppression.

The corresponding results for the right-handed neutrinos are presented in Figs. 3 and 4. The damping rate and thus the parameter coefficients $a_\pm$ depend in this case not

only on the Yukawa coupling but also on the symmetry breaking mass $m_{S,vac} \sim \lambda_M f'$ as well as the on thermal mass $m_{S,th} \sim T$ of the singlet Higgs S, all of which can be viewed as free parameters. We have presented a_+ and a_- as functions of the scalar mass $m_S^2 = m_{S,vac}^2 + m_{S,th}^2$ for some representative values of the Yukawa coupling $g\lambda_M$ and ratio $r = m_M/m_R(T)$, where m_R is the thermal mass and m_M the vacuum mass of the right-handed neutrino. It is noteworthy that the ratio r does not depend on the Yukawa coupling constant but only on the ratio $\bar{f}/T$. It varies in the range from $r = 0$ to $r \simeq 6$, the upper limit corresponding to its value at $\bar{f} \simeq T$.

The damping rates of holes and particles behave quite differently when the parameters are varied, the case of holes showing more structure. The general trend for holes is that the larger r, the larger is the damping rate. This can be seen in Fig. 3 a. However, for each value of r there exists an interval in the values of the ratio $m_S(T)/m_R(T)$ where the damping rate is suppressed. E.g., for $r = 2$ the damping rate is only ~ 0.1 when $m_S(T)/m_R(T)$ lies between values 2 and 3, while outside this range it is some two orders of magnitude larger. This is due to the fact that only soft processes are allowed in this specific parameter region.

Also we find that the damping rate of the holes is quite sensitive to the value of the Yukawa coupling λ_M (Fig. 3 b). The particle damping rate instead depends essentially only on the ratio r. When r increases the damping rate decreases until a threshold mass is reached, as depicted in Figs. 4 a and 4 b. At that threshold the annihilation channel opens which drastically increases the interaction rate. However, the value of λ_M does not affect the damping rate but only marginally. Also for large r the damping rates for the particle-like excitation are generally smaller than for the holes. The main reason is that incoming particles tend to scatter off the holes, and the number density of the holes in the heat bath is suppressed compared with the number density of particles.

6 Conclusions

In the present paper we have studied the thermalization of low momentum neutrinos in the heat bath in the framework of the singlet Majoron model. This is a relevant issue in connection to the charge transport mechanism for generating the baryon asymmetry during the electroweak phase transition [5] when the reflection of neutrinos from the phase wall and from the matter in the broken phase is considered.

We found that the damping rate of the left-handed neutrinos depends only on the temperature corrected vev f of the doublet Higgs field, not on other parameters of the model. This dependence is not particularly strong, the coefficient a defined in Eq. (14) varying between $a = 6$ and $a = 3.5$ when f increases from 0 to $2T$. The result $a \simeq 6$, corresponding to the unbroken gauge symmetry, is quite close to the

value of the corresponding parameter obtained in QCD for quark damping, $a \simeq 5.7$ (for three flavours) [3]. We found the damping rate of the left-handed neutrinos being determined solely by diagrams involving gauge bosons. Therefore our result can, up to some corrections $\mathcal{O}(1)$, be directly generalized to the left-handed charged leptons, too. Furthermore, while the result was derived in the Majoron model, it is valid for the left-handed leptons of the Standard Model as well, since the new degrees of freedom the Majoron model introduces play no role in the leading order calculation.

The damping rates the right-handed neutrinos, which do not couple to the gauge fields, are determined by the Yukawa couplings and properties of the singlet scalar Higgs. Hence the damping rate is more model dependent than in the case of left-handed neutrinos. Depending on the values of various parameters, such as the vacuum mass and the vacuum expectation value of the singlet Higgs, one can find large as well as small damping rates for the right-handed neutrinos.

The present analysis has been performed at the electroweak phase transition temperature $T \simeq 100$ GeV, whereas the QCD calculations of Ref. [3] was performed at QCD phase transition temperature $T = 200$ MeV [1]. On the other hand, in the region where the gauge symmetry is broken, the mass of the weak gauge bosons tends to decrease the damping rate. The net effect is that the rough estimate for the thermalization time, $1/\gamma \sim 0.1(\mathrm{GeV})^{-1}$, used e.g. in [18], is about correct for the left-handed leptons, while the thermalization time of the right-handed neutrinos may differ from this crucially.

For each particle species the damping rate should be smaller than the particle mass. In the opposite case it would be meaningless to speak about particles traversing the medium. In the view were the particle mass is thought to be built up gradually as a result of sequential forward scatterings, particles would in this case decay faster that they are formed. For the right-handed neutrinos this means that the mass given by (23) has to be smaller than the damping rate (29), implying $\lambda_M a_\pm < 4\pi$. This cuts out some large values of $a_\pm$ as unphysical.

A general conclusion of the present paper is that the damping is fairly strong, not only in QCD, but also in the electroweak sector. Hence the reflection probability of the neutrinos may in general be substantially reduced which may crucially affect the charge transport mechanism of the baryon asymmetry generation of the early universe. However, there is a region in the parameter space where the damping rate is suppressed allowing the right-handed neutrinos to penetrate deep into the broken phase.

[1] It is noteworthy that if QCD calculations of Ref. [3] had been performed at the electroweak phase transition temperature, the effective number of degrees of freedom in the heat bath would be increased.

Acknowledgment

This work has been supported by the Academy of Finland and Turun Yliopistosäätiö.

Appendix

In this Appendix we present the derivation of the effective vertices needed for the evaluation of the damping rate of the left-handed neutrinos.

The hard thermal loops which enter into the calculation of the damping rate of the left-handed neutrinos arise from the sums of the form [3, 17]

$$H_n^{\mu_1\cdots\mu_{n-1}} = \mathrm{Tr}\, K^{\mu_1}\cdots K^{\mu_{n-1}} \prod_{i=1}^{n} \left((K+P_i)^2 - m_i^2 \right)^{-1}, \tag{A1}$$

where

$$\mathrm{Tr} = T\sum_{k_0} \int \frac{d^3k}{(2\pi)^3}. \tag{A2}$$

It is understood that the zero component of the momentum attached to a boson (fermion) line is an even (odd) multiple of $\pi T i$, and the momenta P_i are linear combinations of external momenta.

Consider then the effective three-point function of an $SU(2)$ gauge boson and a fermion pair. There are three loops contributing: one with two $SU(2)$ gauge boson propagators and one fermion propagator; one with two fermion propagators and one $SU(2)$ gauge boson propagator; and one with two fermion propagators and one $U(1)$ gauge boson propagator. Extracting the HTL contribution and taking into account the group theoretic factors we obtain in the case of SU(2) gauge bosons

$$\Gamma_2^{\mu,A} = g_2 T^A \left(g^{\mu\nu} + 4C_F^g H_{3;2}^{\mu\nu} \right) \gamma_\nu, \tag{A3}$$

where T^A is an SU(2) generator and $C_F^g = 3/4g_2^2 + Y^2/4g_1^2$ is the Casimir operator of the $(\mathbf{2}, Y)$ representation of $SU(2)\times U(1)$ scaled with the appropriate couplings. In $H^{\mu\nu}$ the first subscript indicates the number of internal lines and the second one denotes the number of fermion propagators. The property $H_{n;m}^{\mu\nu} = -H_{n;n-m}^{\mu\nu}$ was used in derivation of the Eq. (A3). A similar formula is obtained for the effective three-point function Γ_1 of a fermion pair and a $U(1)$ gauge boson:

$$\Gamma_1^{\mu} = g_1 \frac{Y}{2} \left(g^{\mu\nu} + 4C_F^g H_{3;2}^{\mu\nu} \right) \gamma_\nu. \tag{A4}$$

Note that the three-point functions above are of the general form

$$\Gamma_A^{\mu} = F_A \left(g^{\mu\nu} + 4C_F^g H_{3;2}^{\mu\nu} \right) \gamma_\nu, \tag{A5}$$

where F_A denotes the generator of the group in question multiplied by the corresponding coupling.

Consider then four-point function of two gauge bosons and a fermion pair. There are three diagrams (+ crossed channels), contributing: those with one, two and three fermion propagators. Extracting the HTL-contribution, calculating the group theoretic factors and treating the $SU(2)$ and $U(1)$ gauge bosons equally the four-point function may be cast to the form

$$\begin{aligned}\Gamma^{\mu\nu}_{AB} &= -8\left(-[F_A,F_C][F_B,F_C]+F_C\{F_A,F_B\}F_C\right)H^{\mu\nu\lambda}_{4;1}\gamma_\lambda \\ &+ 8\left([F_B,F_C]F_AF_C+[F_A,F_C]F_BF_C\right)H^{\mu\nu\lambda}_{4;2}\gamma_\lambda. \end{aligned} \tag{A6}$$

As will be shown below, when the gauge boson momenta are equal, which is the case in Eq. (5), the HTL-sums are related as

$$H^{\mu\nu\lambda}_{4;1} = -\frac{1}{2}H^{\mu\nu\lambda}_{4;2}. \tag{A7}$$

Inspection shows that the four-point function can be written in this case as

$$\Gamma^{\mu\nu}_{AB} = 4C_F^g\{F_A,F_B\}H^{\mu\nu\lambda}_{4;2}\gamma_\lambda. \tag{A8}$$

The sum in Eq. (A1) is most easily evaluated by applying the formula (see e.g. [12])

$$T\sum_{k_0}F(k_0) = \frac{\eta}{2\pi i}\oint dz f_\eta(z)[F(z)+F(-z)], \tag{A9}$$

where $\eta=-1$ corresponds to the Bose-Einstein and $\eta=+1$ to the Fermi-Dirac distribution, the appropriate distribution chosen according to whether k_0 is even or odd multiple of πTi. The integration path encloses all the poles of the function $F(z)$ on the right half of the z-plane. A calculation results in

$$\begin{aligned}H_n^{\mu_1\cdots\mu_{n-1}} &= \int\frac{d^3k}{(2\pi)^3}\sum_{j=1}^n\eta_j\left\{\mathcal{K}_{|k_0=\omega_j-p_j^0}\frac{f_{\eta_j}(\omega_j)}{2\omega_j}\prod_{i\neq j}\left[(\omega_j-p_j^0+p_i^0)^2-\omega_i^2\right]^{-1}\right. \\ &+ \left.\mathcal{K}_{|k_0=-\omega_j-p_j^0}\frac{f_{\eta_j}(\omega_j)}{2\omega_j}\prod_{i\neq j}\left[(\omega_j+p_j^0-p_i^0)^2-\omega_i^2\right]^{-1}\right\}. \end{aligned} \tag{A10}$$

Here a shorthand notation $\mathcal{K}=K^{\mu_1}\cdots K^{\mu_{n-1}}$ was used and

$$\omega_i = \sqrt{(\mathbf{k}+\mathbf{p}_i)^2+m_i^2}. \tag{A11}$$

Next we perform a linear approximation in external momenta in the denominators and neglect the dependence of the external momenta elsewhere:

$$\begin{aligned}H_n^{\mu_1\cdots\mu_{n-1}} &= \frac{1}{\pi^2 2^{n+1}}\sum_{j=1}^n\eta_j\int_0^\infty dk\,k f_{\eta_j}(k)\times \\ &\int\frac{d\Omega}{4\pi}\left\{\prod_{i\neq j}\frac{\hat{\mathcal{K}}}{(P_i-P_j)\cdot\hat{K}}+\prod_{i\neq j}\frac{\hat{\mathcal{K}}'}{(P_i-P_j)\cdot\hat{K}'}\right\}. \end{aligned} \tag{A12}$$

Here $\hat{K} = (1, +\hat{\mathbf{k}})$, $\hat{K}' = (1, -\hat{\mathbf{k}})$, and the numerator $\hat{\mathcal{K}}$ is defined as $\hat{\mathcal{K}} = \hat{K}^{\mu_1} \cdots \hat{K}^{\mu_{n-1}}$ (and similarly for $\hat{\mathcal{K}}'$). Finally, after the k-integral is performed we end up with

$$H_n^{\mu_1 \cdots \mu_{n-1}} = \frac{T^2}{6 \cdot 2^n} \int \frac{d\Omega}{4\pi} \hat{\mathcal{K}} \left\{ -\sum_{j,B} \prod_{i \neq j} \frac{1}{(P_i - P_j) \cdot \hat{K}} + \frac{1}{2} \sum_{j,F} \prod_{i \neq j} \frac{1}{(P_i - P_j) \cdot \hat{K}} \right\}. \quad \text{(A13)}$$

Here the sum over internal lines is divided to the fermion and boson contributions.

Using the Eq. (A13) and plugging in the appropriate momentum configuration in the function $H_{3;2}^{\mu\nu}$ gives

$$\Gamma_A^\mu = F_A \left(\gamma^\mu + \omega_l^2(T) \int \frac{d\Omega}{4\pi} \frac{\hat{K} \cdot \gamma \hat{K}^\mu}{\hat{K} \cdot P_1 \, \hat{K} \cdot P_2} \right), \quad \text{(A14)}$$

where P_1 (P_2)is the incoming (outgoing) momentum of the fermion and

$$\omega_l(T)^2 = C_F^g \frac{T^2}{8} \quad \text{(A15)}$$

is the thermal mass of the left-handed fermion [14].

The relevant momentum configuration of the function $H_{4;1}$ is $P_1 = P_2 = 0$, $P_3 = -Q$ and $P_4 = P$, where Q is the momentum of the incoming and outgoing gauge boson and P is the momentum of the incoming and outgoing fermion. The term inside the braces in Eq. (A13) may in this case be expressed as

$$\{\ldots\} = \frac{3}{2} \frac{1}{(\hat{K} \cdot P)^2 \, \hat{K} \cdot (P + Q)}. \quad \text{(A16)}$$

On the other hand, the relevant momentum configuration of the function $H_{4;2}$ is $P_1 = 0$, $P_2 = Q$, $P_3 = P$ and $P_4 = P + Q$, and the term inside the braces in Eq. (A13) becomes

$$\{\ldots\} = -\frac{3}{2} \frac{1}{(\hat{K} \cdot P)^2} \left(\frac{1}{\hat{K} \cdot (P - Q)} + \frac{1}{\hat{K} \cdot (P + Q)} \right). \quad \text{(A17)}$$

As the momentum Q is integrated over, and the propagator of the gauge boson is symmetric in Q, one can conclude from (A16) and (A17) that $H_{4;1} = -1/2 H_{4;2}$. The four-point function has then the form

$$\Gamma_{AB}^{\mu\nu} = \omega_l^2(T) \{F_A, F_B\} \int \frac{d\Omega}{4\pi} \frac{\hat{K} \cdot \gamma \hat{K}^\mu \hat{K}^\nu}{(\hat{K} \cdot P)^2 \, \hat{K} \cdot (P + Q)}. \quad \text{(A18)}$$

The effective propagators may be calculated along similar lines. The gauge boson vacuum polarization functions read as

$$\begin{aligned} \Pi_T^{AB} &= \delta^{AB} \Pi_T &&= \delta^{AB} 3M(T)^2 (1 - x^2)(1 - \frac{x}{2} L), \\ \Pi_L^{AB} &= \delta^{AB} \Pi_L &&= \delta^{AB} (\frac{3}{2} M(T)^2 - \frac{1}{2} \Pi_T), \end{aligned} \quad \text{(A19)}$$

where $x = \omega/k$ and $L = \log((1+x)/(1-x))$. The thermal masses for the $SU(2)$ and $U(1)$ gauge bosons are up to the coupling constants equal:

$$\begin{aligned} M^2_{SU(N)} &= \frac{N_f + 4N + 2}{4}\frac{g_2^2 T^2}{9} = \frac{11}{18} g_2^2 T^2 \\ M^2_{U(1)} &= \frac{\sum Y_L^2 + \sum Y_R^2 + 2}{8}\frac{g_1^2 T^2}{9} = \frac{11}{18} g_1^2 T^2. \end{aligned} \tag{A20}$$

Here N_f is the number of left-handed $SU(2)$ doublet fermion representations present in the thermal bath. We have performed the calculations with $N_f = 12$, i.e. the thermal bath is assumed to contain also top quarks. However, the results are not expected to be very sensitive to small variations of N_f or $Y_{L,R}$. The contribution $\frac{2}{8}\frac{g_1^2 T^2}{9}$ in (A20) come from the scalar doublet contribution.

The propagator sum of the gauge bosons may be cast to the form

$$\frac{1}{2g_2^2}\{F_A, F_B\}\Delta^{AB}_{L,T} = \frac{1}{2}\frac{1}{\Gamma_2^{L,T}} + \frac{1}{4}(\Gamma_1^{L,T}\Gamma_2^{L,T} - \Gamma_{12}^2)^{-1}(\Gamma_1^{L,T} + \Gamma_2^{L,T}\tan^2\theta_w + 2\Gamma_{12}\tan\theta_w), \tag{A21}$$

where

$$\begin{aligned} \Gamma_{1,2}^{L,T} &= \omega^2 - k^2 - \Pi_{L,T}^{1,2} - g_{1,2}^2\left(\frac{f}{2}\right)^2, \\ \Gamma_{12} &= g_1 g_2 \left(\frac{f}{2}\right)^2, \end{aligned} \tag{A22}$$

and $\tan\theta_w = g_1/g_2$.

The fermion propagators are of the form

$$\begin{aligned} \Delta_L^{-1} &= \gamma\cdot P - \Sigma_L, \\ \Delta_R^{-1} &= \gamma\cdot P - \Sigma_R - m_M, \end{aligned} \tag{A23}$$

where

$$\Sigma_{L,R}(P) = \omega_{l,r}^2(T)\int\frac{d\Omega}{4\pi}\frac{\hat{K}\cdot\gamma}{\hat{K}\cdot P} = \frac{\omega_{l,r}^2}{2p}\left[L\gamma_0 + (2 - xL)\hat{\mathbf{p}}\cdot\boldsymbol{\gamma}\right], \tag{A24}$$

the notation being the same as in Eq. (A19), ω_l is the thermal mass from Eq. (A20) and ω_r^2 defined in Eq. (21) gives the thermal mass of the right-handed neutrino arising from the scalar-fermion loop.

Using Eqs. (A14), (A18), (A19) and (A24), it is easy to deduce the following Ward identities:

$$\begin{aligned} (P_1 - P_2)_\mu \Gamma_A^\mu(P_1, P_2) &= F_A\left(\Delta_l(P_1)^{-1} - \Delta_l(P_2)^{-1}\right) \\ Q_\mu Q_\nu \Gamma_{AB}^{\mu\nu}(P, Q) &= \{F_A, F_B\}\left(\Delta_l(P+Q)^{-1} - \Delta_l(P)^{-1}\right). \end{aligned} \tag{A25}$$

The latter of these identities holds only in the case where there is an integration over gauge boson momentum Q.

References

[1] See e.g., M. E. Carrington, T. H. Hanson, H. Yamagishi and I. Zahed, Ann. Phys. (N.Y.) **190** (1984) 373 and references therein.

[2] R. D. Pisarski, *Phys Rev. Lett.* **63** (1989) 1129.

[3] E. Braaten and R. D. Pisarski, *Phys. Rev. D* **46** (1992) 1829.

[4] E. Braaten and R. D. Pisarski, *Phys. Rev. D* **42** (1990) 2156; *Nucl. Phys.* **B337** (1990) 569; see also Ref. [17].

[5] A. G. Cohen, D. B. Kaplan and A. E. Nelson, *Nucl. Phys.* **B349** (1991) 727.

[6] M. B. Gavela *et al.* , Mod. Phys. Lett. **A9** (1994) 795; *Nucl. Phys.* **B430** (1994) 382.

[7] P. Huet and E. Sather, *Phys. Rev. D* **51** (1995) 379.

[8] T. Holopainen, J. Maalampi, J. Sirkka and I. Vilja, work in progress.

[9] Y. Chikashige, R. N. Mohapatra and R. D. Peccei, *Phys. Lett.* **B98** (1981) 265, *Phys Rev. Lett.* **45** (1980) 1926.

[10] A. D. Sakharov, JETP Lett. 5 (1967) 24.

[11] K. Enqvist, K. Kainulainen and I. Vilja, *Nucl. Phys.* **B403** (1993) 749.

[12] See, e.g. J. Kapusta, Finite-temperature field theory (Cambridge University Press, Cambridge, 1989).

[13] H. Arthur Weldon, *Phys. Rev. D* **26** (1982) 1394.

[14] H. Arthur Weldon, *Phys. Rev. D* **26** (1982) 2789.

[15] H. Arthur Weldon, *Phys. Rev. D* **40** (1989) 2410.

[16] H. Arthur Weldon, *Phys. Rev. D* **28** (1983) 2007.

[17] J. Frenkel and J. C. Taylor, *Nucl. Phys.* **B334** (1990) 199.

[18] J. Maalampi, J. Sirkka and I. Vilja, *Phys. Lett.* **B 337** (1994) 122.

Figure captions

Figure 1. Generic effective diagrams for the neutrino damping rates: a) diagrams contributing to the left-handed neutrinos, b) diagrams contributing to the right-handed neutrinos and c) non-contributing Diagrams.

Figure 2. Damping rate of the left-handed neutrinos as a function of the vacuum expectation value of the doublet field: the total rate (solid line), contribution coming from particle-hole annihilation (dashed line) and the other contributions (dotted line).

Figure 3. Damping rates of right-handed hole-like excitations of neutrinos as function of the total scalar mass m_S: (a) For Yukawa coupling $\lambda_M = 0.1$ and various ratios $r =$ 0, 2 and 6; (b) For fixed ratio $r = 6$ and for Yukawa couplings $\lambda_M = 0.1$, 0.5, 1.

Figure 4. Damping rates of right-handed particle-like excitations of neutrinos as function of the total scalar mass m_S with ratios $r = 0$, 2: (a) $\lambda_M = 0.1$, (b) $\lambda_M = 1.0$.

Table caption

Table 1. The decay channels of the on-shell contribution to the damping rate of the right-handed particle (γ_+) and hole (γ_-) excitations and corresponding mass thresholds.

Table 1

γ_+	$m_S < \omega_r^+ - \omega_r^-$	$m_S > \omega_r^+ - \omega_r^-$	$m_S > 2\omega_r^+$
	$\nu_p \to S\bar{\nu}_h$	$\nu_p\nu_h \to S$	$\nu_p\bar{\nu}_p \to S$

γ_-	$m_S < \omega_r^+ - \omega_r^-$	$m_S > \omega_r^+ - \omega_r^-$	$m_S > 2\omega_r^-$
	$\bar{\nu}_h S \to \nu_p$	$\bar{\nu}_h\bar{\nu}_p \to S$	$\nu_h\bar{\nu}_h \to S$

Fig. 1 a

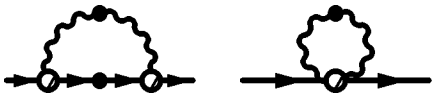

Fig. 1 b

Fig. 1 c

Fig. 2

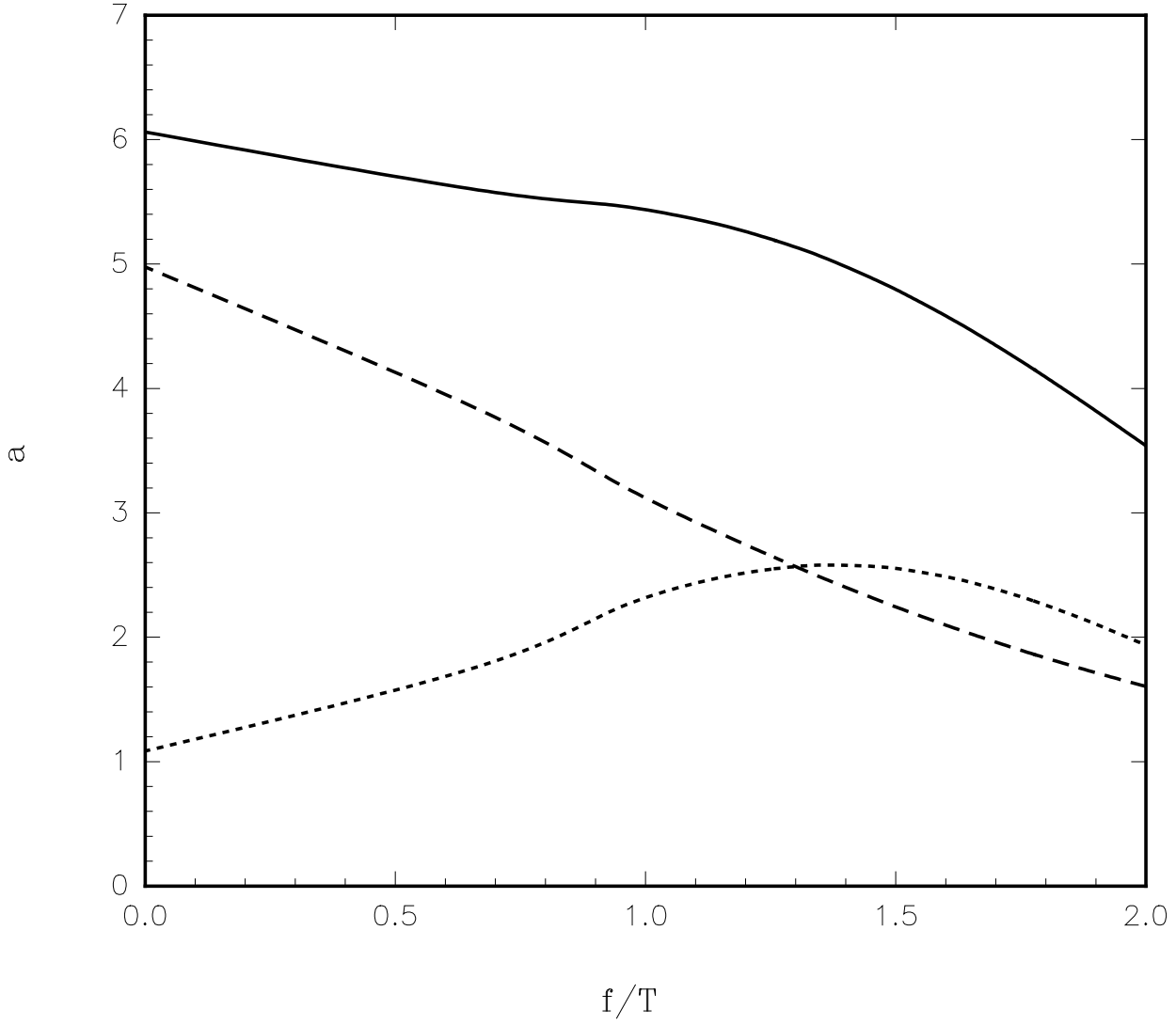

Fig. 3 a

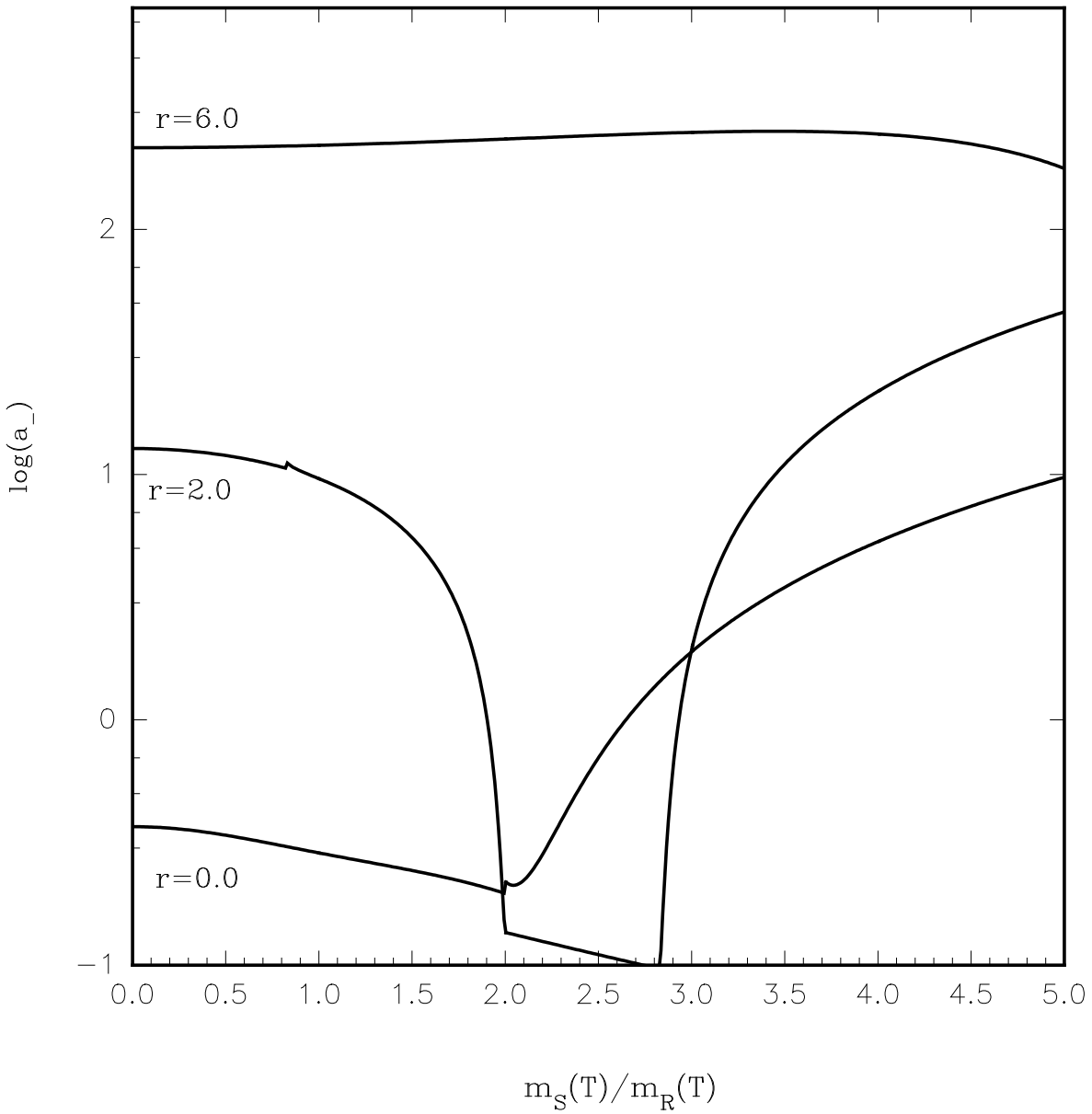

Fig. 3 b

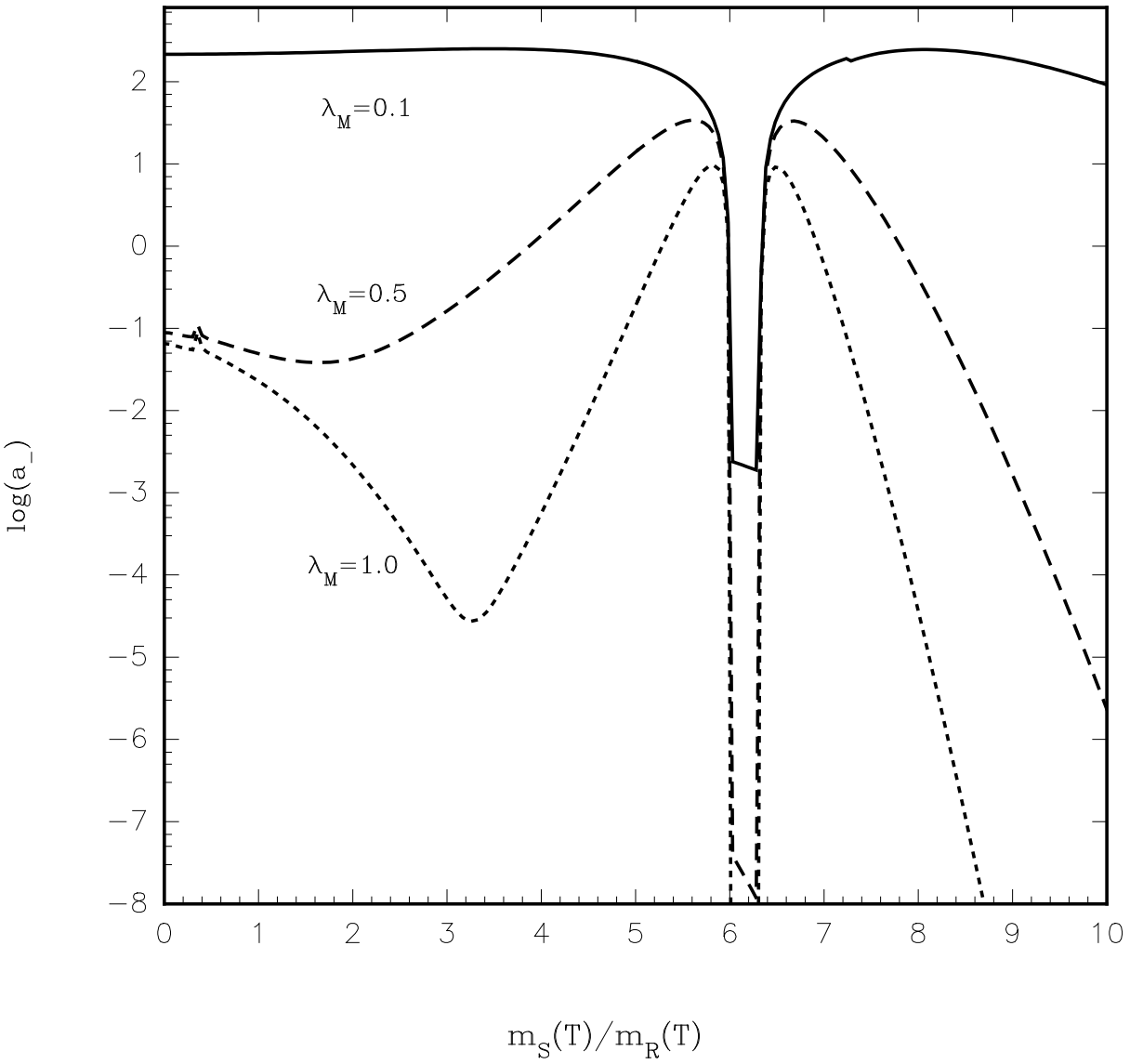

Fig. 4 a

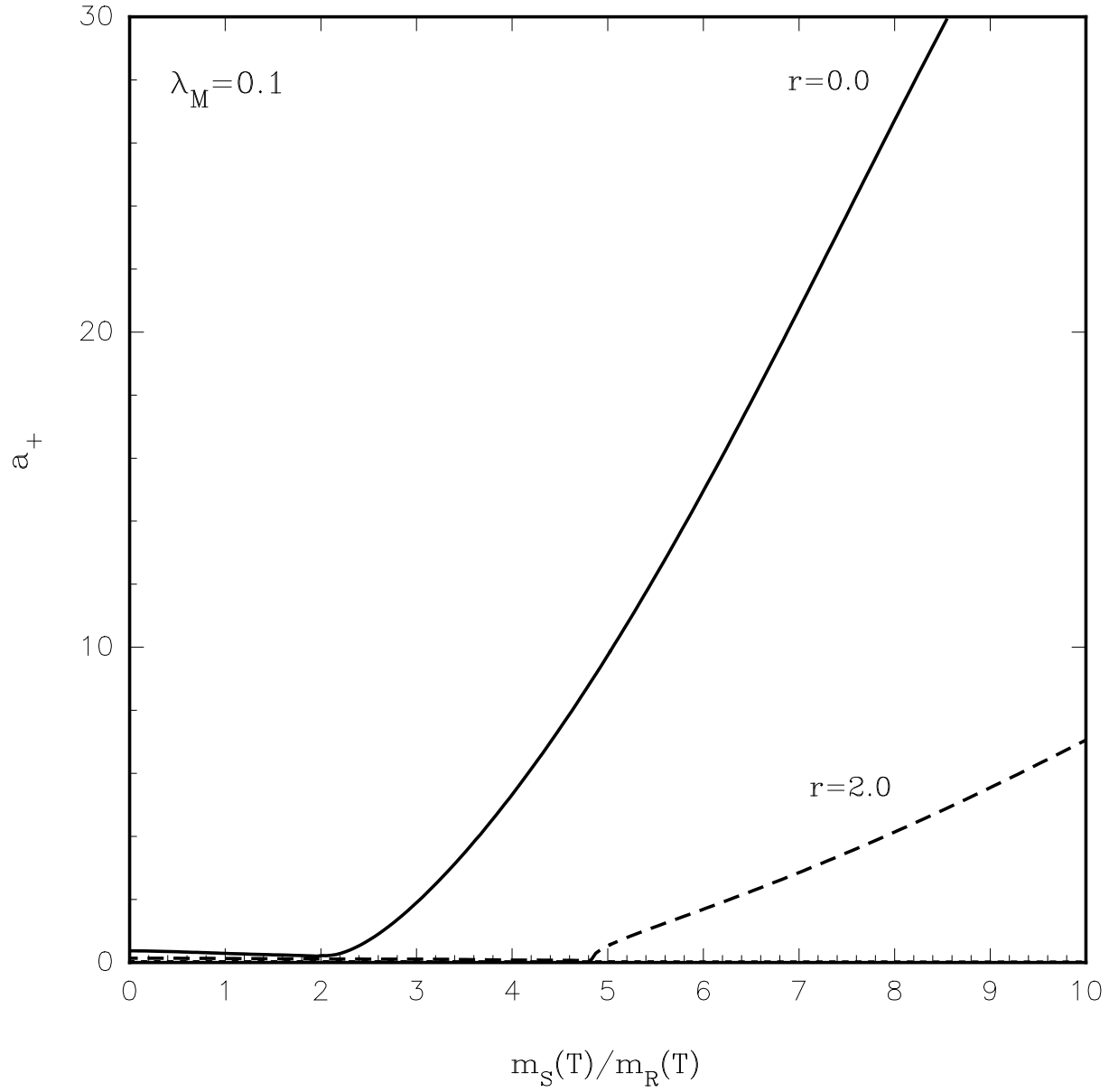

Fig. 4 b